Sustainable Energy & Fuels

Low-cost green synthesis of zinc sponge for rechargeable, sustainable batteries

Journal:	*Sustainable Energy & Fuels*
Manuscript ID	SE-ART-04-2020-000562.R1
Article Type:	Paper
Date Submitted by the Author:	01-May-2020
Complete List of Authors:	Hopkins, Brandon; US Naval Research Laboratory, Chervin, Christopher; US Naval Research Laboratory, Surface Chemistry Branch Sassin, Megan; US Naval Research Laboratory, Surface Chemistry Branch Long, Jeffrey; US Naval Research Laboratory, Surface Chemistry Branch Rolison, Debra; US Naval Research Laboratory, Surface Chemistry Branch Parker, Joseph; US Naval Research Laboratory, Surface Chemistry - Code 6170

Low-cost green synthesis of zinc sponge for rechargeable, sustainable batteries

Brandon J. Hopkins,*[a] Christopher N. Chervin,[b] Megan B. Sassin,[b] Jeffrey W. Long,[b] Debra R. Rolison,*[b] and Joseph F. Parker[b]

[a] Naval Research Laboratory–National Research Council Postdoctoral Associate
Email: brandon.hopkins.ctr@nrl.navy.mil
[b] Surface Chemistry Branch, U. S. Naval Research Laboratory, Code 6170, Washington, DC 20375, USA
Email: debra.rolison@nrl.navy.mil

Policy makers and consumers push for sustainable batteries that rely on abundant, recyclable materials with accessible, stable supply chains. Growing concerns over lithium-ion battery safety, recyclability, and reliance on shrinking cobalt reserves prompt efforts to advance alternative chemistries. To identify promising candidates, we review supply-risk data and the abundance of battery-relevant elements in the Earth's upper continental crust. We find that of the rechargeable-battery chemistries that rely on abundant low-risk elements, zinc (Zn) batteries, namely Zn–MnO_2 and Zn–air, are the lowest cost and most energy dense. Guided by this analysis, we advance Zn batteries by reporting a green synthesis that dramatically lowers the cost and boosts the performance of rechargeable Zn-sponge electrodes. We test these electrode architectures in Zn–air cells and demonstrate a 3,200% increase in rechargeable areal capacity over the majority of previously reported work.

Introduction

While scientists have devoted substantial effort creating batteries that store sustainable energy from wind and solar, many have overlooked the need for these batteries to be sustainable themselves. Most battery chemistries use complex combinations of scarce and impractically expensive metals with high-risk supply chains. Especially when scarce metals are used in small

quantities, recycling comingled metals can be technically or economically infeasible and thus not sustainable.[1,2] For example, most lithium-ion batteries cannot be profitably recycled with existing technologies due to such issues.[2] With this perspective in mind, we seek to identify sustainable, rechargeable batteries and to construct high-performance, low-cost battery electrodes using greener protocols.

Results and discussion

Zinc batteries are sustainable, affordable, and energy dense

To identify sustainable batteries, we plot supply risk[3] of critical elements used in batteries as a function of the abundance of those elements in the Earth's upper continental crust[4] (Fig. 1a). We use supply-risk data from the European Union, noting that different territories have varying supply risk. The 2017 report, written for the European Commission by Deloitte Sustainability and a coalition of European scientists, defines a supply risk less than one as "noncritical" or low.[3] Elements with risk greater than one are prone to high prices and price volatility.[3,5] We define abundant as greater than 0.002 weight percent (wt%) or between the abundance of cobalt (Co), 0.0017 wt%, and lithium (Li), 0.0021 wt%.[4] We base this threshold on the concern that there may be insufficient Co but sufficient Li for vehicle electrification using Li-ion batteries.[5,6] We note that both thresholds indicate gradients of acceptability that rely on variables such as production rates, ore concentrations, geopolitical circumstances, recycling efforts, and battery-materials demand.

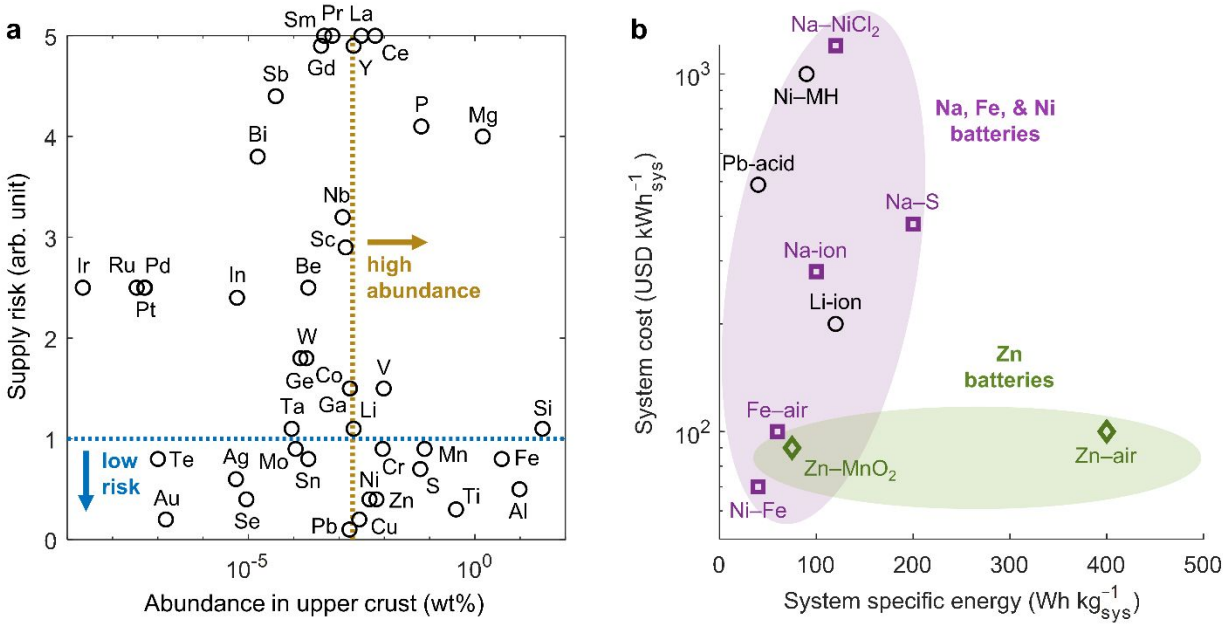

Fig. 1 Zinc batteries are sustainable, affordable, and energy dense. (a) European Union supply risk[3] versus abundance of battery-relevant elements in the Earth's upper continental crust.[4] See also ESI Table 1. (b) System cost versus system specific energy of rechargeable batteries that primarily rely on abundant, low-risk elements as defined by Fig. 1a. Purple: batteries based on sodium (Na), iron (Fe), and/or nickel (Ni). Green: batteries based on Zn. Black: common batteries such as lead-acid (Pb-acid), nickel–metal hydride (Ni–MH), and lithium-ion (Li-ion) that rely on scarce and/or high-risk elements. See also ESI Table 2.

Using these thresholds, we find that the following are abundant, inexpensive, low-risk elements[7–9] (Fig. 1a): nickel (Ni, 14 USD kg^{-1}), chromium (Cr 7.4 USD kg^{-1}), copper (Cu, 5.9 USD kg^{-1}), titanium (Ti, 4.8 USD kg^{-1}), zinc (Zn, 2.5 USD kg^{-1}), manganese (Mn, 2.1 USD kg^{-1}), aluminum (Al, 1.8 USD kg^{-1}), sulfur (S, 0.25 USD kg^{-1}), and iron (Fe, 0.12 USD kg^{-1}). In contrast, Co (80 USD kg^{-1}) and Li (50 USD kg^{-1}) are scarce, expensive, high-risk elements.[7,9] The 2017 report does not provide risk numbers for some abundant elements used in batteries such as calcium (Ca, 2.6 wt%), sodium (Na, 2.4 wt%), potassium (K, 2.3 wt%), fluorine (F, 0.056 wt%), and chlorine (Cl, 0.037 wt%).[4] We assume these elements, along with hydrogen, nitrogen, and carbon, are also low risk based on their abundance and global

production.[10] We note that using global production with a threshold of 10^9 kg y^{-1}, instead of crustal abundance with a threshold of 0.002 wt%, yields a similar short list of elements.[10]

We identify rechargeable batteries with reported system costs and specific energies that rely on the identified elements and find that Zn batteries are the lowest cost and most energy dense (Fig. 1b).[11–21] Rechargeable air-breathing electrodes in alkaline electrolyte can be constructed using abundant, low-risk compounds such as polymorphs of MnO_2 for oxygen reduction[22,23] and mixed oxides, hydroxides, or oxyhydroxides of Ni and Fe for oxygen evolution.[24–26] We exclude flow batteries from this analysis as they are not optimized for specific energy, and their cost is primarily controlled by tank size.[27,28] This analysis generally shows that batteries based on Na, Fe, and Ni have high cost-to-specific-energy ratios while Zn–MnO_2 (alkaline and Zn-ion) and Zn–air have low cost-to-specific-energy ratios (Fig. 1b). Such Zn batteries are also desirable because they use nonflammable aqueous electrolytes. Historically, batteries with a Zn electrode provided limited cycle life, but recent advances, such as the dendrite-suppressing Zn-sponge electrode,[29–32] have yielded substantial rechargeability improvements, contributing to an accelerated productivity and interest in Zn batteries (ESI Fig. 1).

Low-cost green synthesis of Zn sponge

We present a green synthesis for Zn sponge that reduces materials cost by 74% to 2.5 USD kg^{-1}. Previously reported protocols to fabricate Zn sponge require a cost-prohibitive polymer-resin porogen that accounts for at least 73% of the materials cost of 9.7 USD kg^{-1} (ESI Fig. 2). Such resins, typically carboxymethyl cellulose (CMC), are regarded as critical for creating emulsion-based Zn sponges.[29–33] We now show that no emulsion is required for synthesis, obviating the need

for hazardous hydrocarbons. We also show that corn starch (0.3 USD kg^{-1}) is a superior substitute for polymer-resin porogen (CMC: 420 USD kg^{-1}).[34]

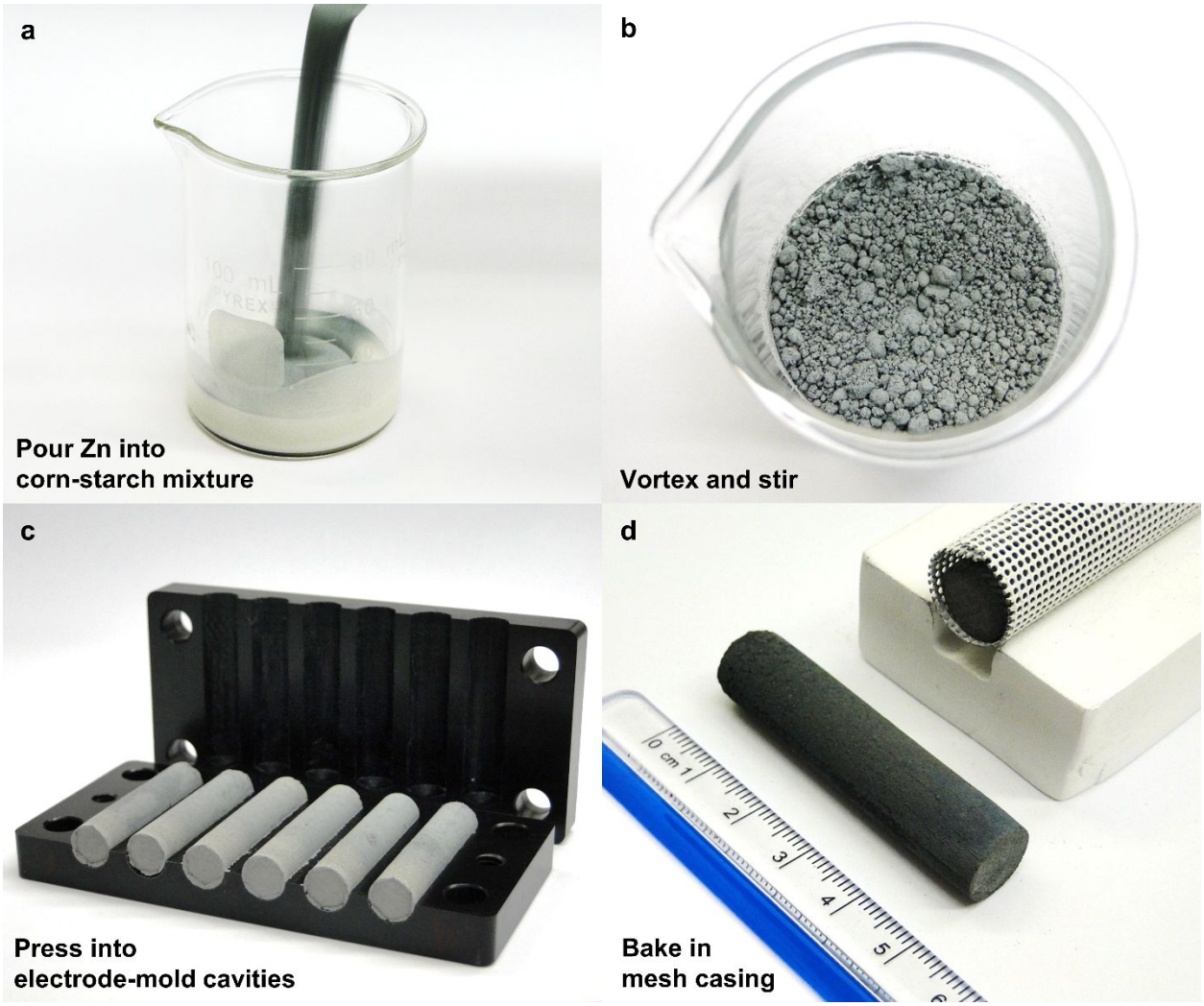

Fig. 2 Low-cost green synthesis of Zn sponge. (a) Pour Zn powder into a mixture containing water, corn starch, and cellulose gum. (b) Vortex while stirring the mixture. (c) Press the Zn paste into electrode-mold cavities. (d) Place dried preforms into a mesh casing for baking: (center) baked 5 cm–long Zn sponge; (right) mesh casing filled with Zn sponges.

The low-cost green synthesis of Zn sponge consists of four steps, which require no humidity control for fabrication, unlike lithium-based chemistries. First, water, corn starch, cellulose gum, and Zn powder are mixed together (Fig. 2a). Corn starch acts as the porogenic filler

and burns out during baking to yield a void network throughout the volume of the sponge. Cellulose gum acts as a thickener that suspends the Zn particles in the aqueous mixture. Second, the mixture is vortexed and stirred (Fig. 2b). Third, the resulting Zn paste is pressed into the cavities of the mold (Fig. 2c). Here, we make Zn sponges with a form factor relevant for AA batteries. Other cavity shapes can be accommodated by machining the Zn sponge directly or by modifying the mold. The mold is heated at 60 °C to dry the Zn paste and to expand the cavities for demolding the Zn-paste preforms. Fourth, the dried Zn preforms are transferred to a mesh casing suspended by a notched alumina block for baking in a tube furnace under nitrogen (N_2) and air (Fig. 2d).[32] The suspended mesh casing enables uniform baking of the sponge cylinders.

Corn starch is a superior porogenic substitute for expensive polymer resin

We show that Zn sponges made using this green protocol yield similar or superior performance to previously reported $Zn_{2.8}$ sponges,[32] which are synthesized using conventional, cost-prohibitive CMC. The 2.8 denotes density, i.e., the sponge has a density of 2.83 ± 0.09 g cm^{-3}. The Zn sponge created using the green synthesis has a higher density of 3.26 ± 0.10 g cm^{-3} and is referred to as "$Zn_{3.3}$." We note that Zn-sponge density and consequently performance can be tuned by adding more or less porogen to the Zn-paste mixture (Fig. 1a).[31–33]

We select off-the-shelf corn starch as a porogen substitute for polymer resin because of its particle size and burnout profile. The corn starch particles are 10 μm in diameter and approximately the same size as the thickness of the CMC polymer–resin branches (Fig. 3a,b). In contrast, the average size of the Zn particles is 50 μm in diameter. The corn starch burns out under the baking protocol used for Zn-sponge synthesis as verified by thermogravimetric analysis (Fig. 3c). After baking, 16% of a CMC residue remains while only 4% of corn starch char remains (Fig.

3c). A higher percentage of porogen char in the Zn sponge is undesirable because the carbonaceous residue can clog the pores of the sponge and reduce useable capacity and power. We note that other food-based or food-waste porogens may be suitable. For example, in early prototypes of the $Zn_{3.3}$ sponge, we found that ball-milled spent coffee grounds act as a suitable porogen, but we used off-the-shelf corn starch to avoid preprocessing.

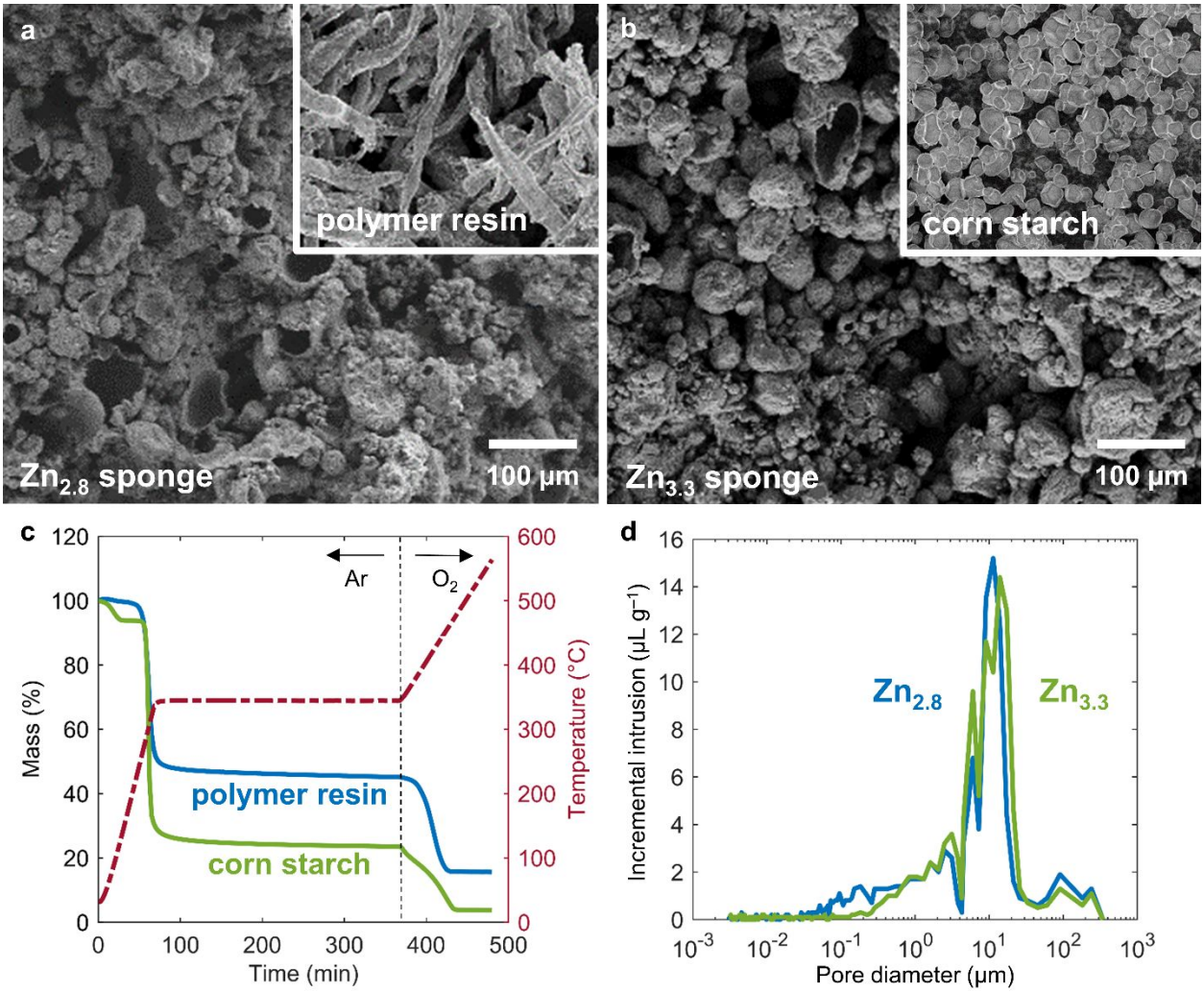

Fig. 3 Corn starch is a superior porogenic substitute for expensive CMC polymer resin. (a) Scanning electron micrograph (SEM) of a cross-sectioned $Zn_{2.8}$ sponge and CMC polymer resin (top right). (b) SEM of a cross-sectioned $Zn_{3.3}$ sponge and corn starch (top right). The scale bars refer to both sponge and porogen images (a,b). (c) Percentage mass and temperature versus time measured by thermogravimetric analysis for the porogens, CMC resin and corn starch, used to create $Zn_{2.8}$ and $Zn_{3.3}$ sponges, respectively. The thermogravimetric analysis, patterned after the Zn-sponge baking protocol, starts under argon (Ar) and

then switches to a mixture of Ar and oxygen (O_2) to mimic air. (d) Incremental intrusion versus pore-size diameter measured via mercury intrusion for representative $Zn_{2.8}$ and $Zn_{3.3}$ sponges.

After verifying that corn starch meets the desired sizing and burnout properties, we find that the $Zn_{2.8}$ and $Zn_{3.3}$ sponges have comparable total pore volumes of 0.13 mL g^{-1} and pore-diameter distributions centered on 10 μm (Fig. 3d) as determined using mercury-intrusion porosimetry. The fact that both pore-diameter distributions peak at 10 μm suggests that the characteristic dimension of the porogen governs pore size in the sponge. If no porogen is added, the Zn particles fuse to form a minimally porous Zn cylinder.

Mechanical and electrochemical performance of $Zn_{3.3}$ sponge

To ensure that the performance of the $Zn_{3.3}$ sponge is similar or superior to the previously tested $Zn_{2.8}$ sponge,[32] we measure mechanical properties and find that the $Zn_{2.8}$ and $Zn_{3.3}$ sponges have comparable tensile strength of 1.1±0.2 MPa and 1.2±0.2 MPa (ESI Fig. 3) and compressive strength of MPa 7.6±0.2 MPa and 7.1±2.0 MPa (ESI Fig. 4), respectively.[35]

We compare power performance in silver–zinc (Ag–Zn) cells and find that 1 mm–thick $Zn_{2.8}$ and $Zn_{3.3}$ sponges achieve peak powers of 134±8 mW cm_{geo}^{-2} and 199±6 mW cm_{geo}^{-2} (per geometric surface area), respectively (Fig. 4b; ESI Fig. 5). We use Ag–Zn cells because the silver electrode can match the high-rate capability of the Zn sponge. We primarily attribute the higher power of $Zn_{3.3}$ to its thinner ZnO shell. Using mercury-intrusion porosimetry, we find that the $Zn_{2.8}$ and $Zn_{3.3}$ sponges have respective specific surface areas of 3.9 and 4.0 $m^2 g^{-1}$ at an absolute pressure of 412 MPa. The $Zn_{3.3}$ sponge has a higher ratio of Zn to zinc oxide (Zn:ZnO) than $Zn_{2.8}$ (as determined using X-ray diffraction; ESI Fig. 6). The Zn content is 72 and 78% for $Zn_{2.8}$ and $Zn_{3.3}$, respectively, with ZnO as the remaining percentage. These data suggest that $Zn_{3.3}$ has a

thinner ZnO shell and a larger cross-sectional area of metallic Zn throughout the volume of the sponge, which enables higher electronic conductivity. The corn starch–derived $Zn_{3.3}$ sponge also has less passivating porogenic residue at its surface (Fig. 3c). We note that a specific surface area of 4.0 $m^2\,g^{-1}$ limits corrosion reactions at the sponge and yields a minimal self-discharge rate of 1% y^{-1}.[32] The measured corrosion rate is low in part because the majority of the electrolyte is stored in the pores of the Zn sponge and quickly becomes saturated with zincate, which slows corrosion.

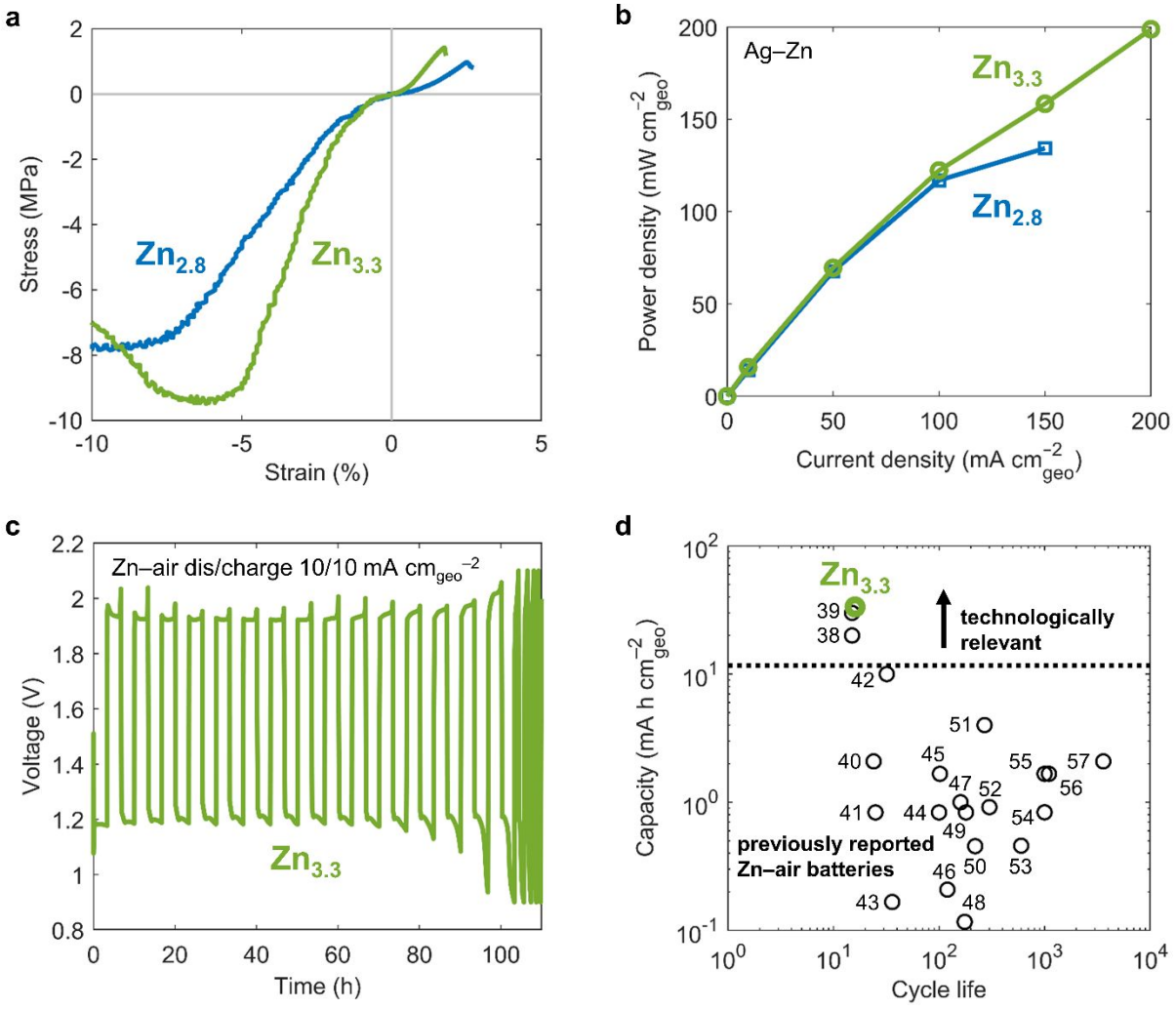

Fig. 4 Mechanical and electrochemical performance of $Zn_{3.3}$ sponge. (a) Stress versus strain of $Zn_{2.8}$ and $Zn_{3.3}$ sponges. See also ESI Figs. 3 and 4. (b) Power versus current density of silver–zinc (Ag–Zn) cells using $Zn_{2.8}$ and $Zn_{3.3}$ electrodes. See also ESI Fig. 5. (c) Voltage versus time of a Zn–air cell using a $Zn_{3.3}$

electrode cycled at 10 mA cm_{geo}^{-2}. (d) Rechargeable areal capacity versus cycle life for this work ($Zn_{3.3}$) and those found in the literature noted by their reference. See also ESI Table 3.

To verify that the $Zn_{3.3}$ sponge retains dendrite-suppressing capabilities, we cycle the $Zn_{3.3}$ sponge in a Ni–Zn cell for 100 cycles at 20 mA cm_{geo}^{-2} to 10% depth of discharge with respect to the total amount of elemental Zn in the cell (DOD_{Zn}) (ESI Fig. 7). We observe no dendrites by SEM after this cycling protocol (ESI Fig. 8). Even when charging the cell at global current densities above those shown to sprout dendrites,[36] the low local current density of 0.002 mA cm_{act}^{-2} (per actual surface area of sponge) suppresses dendrite formation.

We then test the $Zn_{3.3}$ sponge in a Zn–air cell, projected to be the lowest cost and most energy dense of the sustainable batteries (Fig. 1b). Cycling the sponge versus a bifunctional air-breathing cathode containing aerogel-based electrocatalysts (Ni_2FeO_x[26] and MnO_2[37]) at 10 mA cm_{geo}^{-2} for 16 cycles to 33.4 mA h cm_{geo}^{-2} delivers a 3,200% increase in rechargeable areal capacity over the majority of previously reported work (Fig. 4c,d).[38–57] At this cycling capacity, which maps to 21% DOD_{Zn}, we observe no dendrites using an electrolyte volume of 0.3 to 0.4 mL in the cell (ESI Fig. 9).

We exclude from Fig. 4d those literature values derived from reports that use air-breathing electrodes containing scarce, high-risk elements as defined by Fig. 1a. Most reported Zn–air cells that demonstrate a high cycle count do so at areal capacities near 1 mA h cm_{geo}^{-2} (Fig. 4d), which is far below the technologically relevant value[13] of 11.7 mA h cm_{geo}^{-2}. We partially attribute these low capacities to the poor rechargeable areal capacity of the zinc foil or powder-composite electrode commonly used in such studies. The two reported Zn–air batteries that achieved technological relevance for areal capacity operated for 30 and 90 h, but because these reports focused on catalyst design, details associated with DOD_{Zn} and electrolyte volume were not

included.[38,39] Both parameters are required to assess Zn–air-cell practicality. In contrast, the Zn–air cell reported here lasts for 107 h before capacity loss and uses practical quantities of Zn and electrolyte. As the performance of positive electrodes improve, $Zn_{3.3}$-sponge electrodes pave the way for sustainable, rechargeable, energy-dense batteries.

Experimental

$Zinc_{3.3}$-sponge synthesis

A mass of 0.120 ± 0.001 g of high viscosity [1500–3000 cP, 1 wt% in H_2O at 25 °C] cellulose gum also known as carboxymethylcellulose (CMC) sodium salt (MilliporeSigma, CAS# 9004-32-4) was added to 10.5 mL of deionized water. This mixture was vortexed and stirred by hand for 5 min. A mass of 2.400 ± 0.001 g of corn starch (Argo 100% pure corn starch) was added to the mixture and vortexed while stirring by hand for 2 min. A mass of 120.00 ± 0.01 g of Zn powder (EverZinc) was added to the mixture and stirred and vortexed for 2 min. Zinc powder was used that consisted of mostly solid, globular particles with an average diameter of 50 μm (89.2% of particles < 75 μm and 0% of particles > 250 μm, containing 307 ppm of bismuth and 307 ppm of indium). This mixture was pressed into mold cavities. The Zn paste was left in the cavities to dry out at 60 °C overnight. The mold was machined from Delrin® acetal (polyoxymethylene also known as POM). The dried Zn paste preform was easiest to demold when the mold was warm. In addition, unsalted butter can act as a mold release that can be applied before the Zn paste is pressed into the mold. The preform was then transferred to the baking mesh shown in Fig. 2d and heated in a tube furnace as previously reported.[32] We note that the first portion of the baking occurred under N_2. After 367 min, the temperature ramped up (Fig. 3c) and air was piped into the tube furnace. We also note that to create a more sustainable sponge, bismuth and indium could be eliminated and a gel or polymer electrolyte could aid in corrosion suppression when alkaline electrolytes are desired. We used doped Zn particles out of laboratory convenience.

Diametral and uniaxial compression tests

Diametral and uniaxial compression tests were performed using a constant displacement of 1 mm min^{-1}. The surfaces of the crushing plates were not lubricated. The diameter of cylindrical

samples used in both tests was 11.5 mm with thickness of 4 mm for uniaxial and diametral compression.

Battery-cell fabrication

Silver–Zn and Ni–Zn cells were assembled as previously reported.[32] Zinc–air cells used tin-foil current collectors on the Zn-electrode side and a platinum or nickel wire current collector on the air-breathing electrode side. The electrolyte was 9 M KOH. One layer of Celgard® 3501 was placed on the Zn-electrode side with one layer of 700/28 Freudenberg separator on the air-breathing electrode side. We note that we used tin and platinum as current collectors for laboratory convenience, but more sustainable options are available. For example, a Zn or carbon-based current collector could be used for the Zn electrode and a Ni current collector could be used for the air-breathing electrode. All battery cells reported in this work used 0.3 to 0.4 mL of electrolyte.

Air-breathing electrode fabrication

Air-breathing electrodes were fabricated as a layered, pressed pellet comprising a catalyst layer, a nickel-foam current collector, and a gas-diffusion layer (GDL). The catalyst layer was made from a 50/50 wt% catalyst mixture of Ni_2FeO_x aerogel and MnO_x aerogel, acetylene black carbon (Cabot) as a conductive component, and PTFE binder (60 wt% dispersion in H_2O) using a 20/65/15 weight ratio of catalyst/conductive carbon/PTFE. The methods we used to fabricate Ni_2FeO_x and MnO_x aerogels are reported in the literature.[26,37] The Ni_2FeO_x aerogel was heated at 275 °C in flowing Ar for 4 h under a 2 °C min^{-1} ramp before incorporation into the catalyst layer. The cryptomelane-type MnO_x was calcined at 300 °C in air for 4 h under a 2 °C min^{-1} ramp.[37]

To prepare the air-breathing electrode catalyst layer, 0.05 g of Ni_2FeO_x and 0.05 g of MnO_x were combined with 0.33 g of carbon, 0.127 g of 60 wt% PTFE aqueous dispersion, and 5 mL of water in an agate ball mill along with 13.5 g of agate mill media. The mixture was milled in a Fritsch Pulverisette 7 mill at 300 rpm in three 15-min intervals with a 5-min rest between each interval. The resulting mixture was collected in a beaker using ethanol to rinse the media and mill and then dried at 70 °C overnight in static air to produce a composite powder. The GDL was prepared in a similar fashion using a 70/30 weight ratio of acetylene black to PTFE. The dried composite catalyst layer and GDL were weighed into 0.050 g portions and a nickel mesh was sandwiched between the two portions in a 1-cm^2 die. The composites were pressed at 20.7 MPa for 1 min to form a 0.8-mm–thick, circular gas-diffusion electrode.

Conflicts of interest

J.F.P., D.R.R., and J.W.L. hold patents related to zinc electrodes: US Patents no. 9802254 and 10008711, EU Patent no 2926395, and China Patent no. 104813521.

Acknowledgements

This research was supported by the U. S. Office of Naval Research.

Footnotes

† Electronic supplementary information (ESI) is available.

References

1. B. K. Reck and T. E. Graedel, *Science*, 2012, **337**, 690–695.
2. G. Harper, R. Sommerville, E. Kendrick, L. Driscoll, P. Slater, R. Stolkin, A. Walton, P. Christensen, O. Heidrich, S. Lambert, and A. Abbott, *Nature*, 2019, **575**, 75–86.
3. S. Soleille, M. A. Kong, M. Planchon, N. Saidi, C. Devauze, E. Petavratzi, G. Gunn, T. Brown, R. Shaw, G. Lefebvre, M. Le Gleuher, E. Rietveld, J. de Jong, T. Nijland and T. Bastein, *Study on the Review of the List of Critical Raw Materials*, Publications Office of the European Union, Luxembourg, 2017, DOI: 10.2873/876644.
4. R. L. Rudnick and S. Gao, *Treatise on Geochemistry 2nd Edition*, Elsevier, 2014, DOI: 10.1016/B0-08-043751-6/03016-4.
5. E. A. Olivetti, G. Ceder, G. G. Gaustad and X. Fu, *Joule*, 2017, **1**, 229–243.
6. K. Turcheniuk, D. Bondarev, V. Singhal and G. Yushin, *Nature*, 2018, **559**, 467–470.
7. Metalary, https://www.metalary.com, (accessed 2019).
8. Fastmarkets MB, https://www.metalbulletin.com/Article/3586680/Chromium-prices-tighten-as-ore-costs-rise.html, (accessed 2019).
9. Z. Li, M. S. Pan, L. Su, P. C. Tsai, A. F. Badel, J. M. Valle, S. L. Eiler, K. Xiang, F. R. Brushett and Y.-M. Chiang, *Joule*, 2017, **1**, 306–327.
10. P. C. K. Vesborg and T. F. Jaramillo, *RSC Adv.*, 2012, **2**, 7933–7947.
11. J. O. G. Posada, A. J. Rennie, S. P. Villar, V. L. Martins, J. Marinaccio, A. Barnes, C. F. Glover, D. A. Worsley and P. J. Hall, *Renew. Sust. Energy Rev.*, 2017, **68**, 1174–1182.
12. N. D. Ingale, J. W. Gallaway, M. Nyce, A. Couzis and S. Banerjee, *J. Power Sources*, 2015, **276**, 7–18.
13. J. F. Parker, J. S. Ko, D. R. Rolison and J. W. Long, *Joule*, 2018, **2**, 2519–2527.
14. S. R. Narayanan, G. S. Prakash, A. Manohar, B. Yang, S. Malkhandi and A. Kindler, *Solid State Ionics*, 2012, **216**, 105–109.
15. S. B. Sherman, Z. P. Cano, M. Fowler and Z. Chen, *Aims Energy*, 2018, **6**, 121–145.
16. N. Zhang, F. Cheng, J. Liu, L. Wang, X. Long, X. Liu, F. Li and J. Chen, *Nature Commun*, 2017, **8**, article no. 405.
17. I. Y. L. Hsieh, M. S. Pan, Y.-M. Chiang and W. H. Green, *Appl. Energy*, 2019, **239**, 218–224.
18. K. G. Gallagher, S. Goebel, T. Greszler, M. Mathias, W. Oelerich, D. Eroglu and V. Srinivasan, *Energy Environ. Sci.*, 2014, **7**, 1555–1563.
19. C. Vaalma, D. Buchholz, M. Weil and S. Passerini, *Nature Rev. Mater.*, 2018, **3**, 18013.
20. B. Zakeri and S. Syri, *Renew. Sust. Energy Rev.*, 2015, **42**, 569–596.
21. L. Ouyang, J. Huang, H. Wang, J. Liu and M. Zhu, *Mater. Chem. Phys.*, 2017, **200**, 164–178.
22. B. J. Hopkins, PhD thesis, Massachusetts Institute of Technology, 2018.
23. B. J. Hopkins, Y. Shao-Horn, D. P. Hart, *Science*, 2018, **362**, 658–661.
24. C. N. Chervin, P. A. DeSario, J. F. Parker, E. S. Nelson, B. W. Miller, D. R. Rolison and J. W. Long, *ChemElectroChem*, 2016, **3**, 1369–1375.
25. C. N. Chervin, J. F. Parker, E. S. Nelson, D. R. Rolison and J. W. Long, *Nanotechnology*, 2016, **27**, 174002.
26. J. S. Ko, C. N. Chervin, M. N. Vila, P. A. DeSario, J. F. Parker, J. W. Long and D. R. Rolison, *Langmuir*, 2017, **33**, 9390–9397.
27. B. J. Hopkins, Master's thesis, Massachusetts Institute of Technology, 2013.
28. X. Chen, B. J. Hopkins, A. Helal, F. Y. Fan, K. C. Smith, Z. Li, A. H. Slocum, G. H. McKinley, W. C. Carter and Y.-M. Chiang, *Energ. Environ. Sci*., 2016, **9**, 1760–1770.
29. J. F. Parker, C. N. Chervin, E. S. Nelson, D. R. Rolison and J. W. Long, *Energy Environ. Sci.*, 2014, **7**, 1117–1124.
30. J. F. Parker, C. N. Chervin, I. R. Pala, M. Machler, M. F. Burz, J. W. Long and D. R. Rolison, *Science*, 2017, **356**, 415–418.
31. J. S. Ko, A. B. Geltmacher, B. J. Hopkins, D. R. Rolison, J. W. Long and J. F. Parker, *ACS Appl. Energy Mater.*, 2018, **2**, 212–216.
32. B. J. Hopkins, M. B. Sassin, C. N. Chervin, J. F. Parker, J. W. Long and D. R. Rolison, *Energy Storage Mater.*, 2020, **27**, 370–376.
33. J. F. Drillet, M. Adam, S. Barg, A. Herter, D. Koch, V. Schmidt, and M. Wilhelm, *ECS Trans.*, 2010, **28**, 13–24.
34. BiopHoretics, https://biophoretics.com/cm-deae-ion-exchange-media-/540-cmc-52-preswollen-carboxymethyl-cellulose.html, (accessed 2019).
35. M. F. Ashby, T. Evans, N. A. Fleck, J. W. Hutchinson, H. N. G. Wadley and L. J. Gibson, *Metal Foams: A Design Guide*, Elsevier, 2000.

36. V. Yufit, F. Tariq, D. S. Eastwood, M. Biton, B. Wu, P. D. Lee and N. P. Brandon, *Joule*, 2019, **3**, 485–502.
37. J. S. Ko, J. F. Parker, M. N. Vila, M. A. Wolak, M. B. Sassin, D. R. Rolison and J. W. Long, *J. Electrochem. Soc*., 2018, **165**, H777–H783.
38. H. B. Yang, J. Miao, S. F. Hung, J. Chen, H. B. Tao, X. Wang, L. Zhang, R. Chen, J. Gao, H. M. Chen, L. Dai and B. Liu, *Sci. Adv*., 2016, **2**, e1501122.
39. A. Sumboja, X. Ge, F. W. T. Goh, B. Li, D. Geng, T. S. A. Hor, Y. Zong and Z. Liu, *ChemPlusChem*, 2015, **80** (8), 1341–1346.
40. K. Marcus, K. Liang, W. Niu and Y. Yang, *J. Phys. Chem. Lett*., 2018, **9**, 2746–2750.
41. S. Chen, J. Duan, Y. Zheng, X. Chen, X. W. Du, M. Jaroniec, S. Z. Qiao, *Energy Storage Mater*., 2015, **1**, 17–24.
42. A. Sumboja, J. Chen, Y. Zong, P. S. Lee and Z. Liu, *Nanoscale*, 2017, **9**, 774–780.
43. Q. Liu, Y. Wang, L. Dai and J. Yao, *Adv. Mater.*, 2016, **28**, 3000–3006.
44. H. Wu, J. Wang, G. Wang, F. Cai, Y. Ye, Q. Jiang, S. Sun, S. Miao and X. Bao, *Nano Energy*, 2016, **30**, 801–809.
45. F. Meng, H. Zhong, J. Yan and X. Zhang, *Nano Res.*, 2017, **10**, 4436–4447.
46. D. Chen, J. Ji, Z. Jiang, M. Ling, Z. Jiang and X. Peng, *J. Power Sources*, 2020, **450**, 227660.
47. B. Li, D. Geng, X. S. Lee, X. Ge, J. Chai, Z. Wang, J. Zhang, Z. Liu, T. S. A. Hor and Y. Zong, *Chem. Commun.*, 2015, **51**, 8841–8844.
48. A. Sumboja, M. Lübke, Y. Wang, T. An, Y. Zong and Z. Liu, *Adv. Energy Mater.*, 2017, **7**, 1700927.
49. Y. Fan, S. Ida, A. Staykov, T. Akbay, H. Hagiwara, J. Matsuda, K. Kaneko and T. Ishihara, *Small*, 2017, **13**, 1700099.
50. L. Ma, S. Chen, Z. Pei, Y. Huang, G. Liang, F. Mo, Q. Yang, J. Su, Y. Gao, J. A. Zapien and C. Zhi, *ACS Nano*, 2018, **12**, 1949–1958.
51. A. Sumboja, X. Ge, G. Zheng, F. W. T. Goh, T. S. A. Hor, Y. Zong and Z. Liu, *J. Power Sources*, 2016, **332**, 330–336.
52. Z. Pei, H. Li, Y. Huang, Q. Xue, Y. Huang, M. Zhu, Z. Wang and C. Zhi, *Energy Environ. Sci.*, 2017, **10**, 742–749.
53. L. Ma, S. Chen, D. Wang, Q. Yang, F. Mo, G. Liang, N. Li, H. Zhang, J. A. Zapien and C. Zhi, *Adv. Energy Mater*., 2019, **9**, 1803046.
54. C. Lin, X. Li, S. S. Shinde, D. H. Kim, X. Song, H. Zhang and J. H. Lee, *ACS Appl. Energy Mater.*, 2019, **2**, 1747–1755.
55. Y. Chen, I. Kone, Y. Gong, A. Xie, H. Hu, D. Kong, J. Liu, Y. Tang, X. Yang, R. Pang and P. Wan, *Carbon*, 2019, **152**, 325–334.
56. X. Xiao, X. Li, Z. Wang, G. Yan, H. Guo, Q. Hu, L. Li, Y. Liu, and J. Wang. *Appl. Catal. B*, **265**, 118603.
57. S. S. Shinde, C. H. Lee, J. Y. Jung, N. K. Wagh, S. H. Kim, D. H. Kim, C. Lin, S. U. Lee and J. H. Lee, *Energy Environ. Sci.*, 2019, **12**, 727–738.

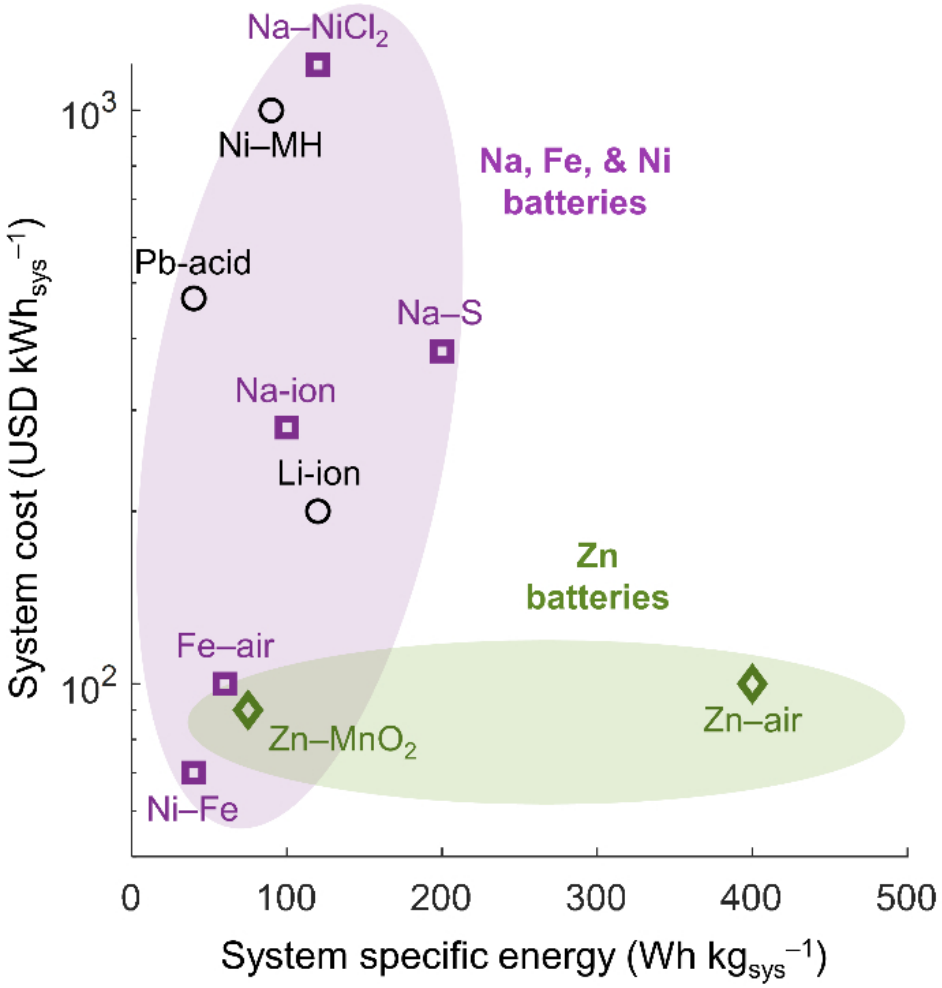

84x84mm (220 x 220 DPI)